Journal of Physical Science Vol. 36(3), 75–87, 2025



Spectroscopic Investigation of Plasma Parameters in an CdO Target Using Laser-Induced Breakdown Spectroscopy

Saeed N. Turki AlRashid, Sabah N. Mazhir^{2*} and Nagham M. Hamid¹

¹Department of Physics, College of Education for Pure Science, University Anbar, Ramadi, Iraq

²Department of Physics, College of Sciences for Women, University of Baghdad, 10072 Baghdad, Iraq

*Corresponding author: sabahnm_phys@csw.uobaghdad.edu.iq

Published online: 28 November 2025

To cite this article: AlRashid, S. N. T. et al. (2025). Spectroscopic investigation of plasma parameters in an CdO target using laser-induced breakdown spectroscopy. *J. Phys. Sci.*, 36(3), 75–87. https://doi.org/10.21315/jps2025.36.3.6

To link this article: https://doi.org/10.21315/jps2025.36.3.6

ABSTRACT: This study investigates the plasma parameters of a cadmium oxide (CdO) target using laser-induced breakdown spectroscopy (LIBS). The plasma spectra of CdO were observed after preparation using a pulsed laser with energies of (300, 500 and 700) mJ. The experiment used a high-power laser to ablate the cadmium (Cd) target, generating a plasma plume that emitted characteristic spectral lines. We extracted valuable information about the plasma parameters by analysing the emitted light, including electron temperature, electron density and ionisation degrees. The LIBS setup was carefully calibrated and optimised to ensure accurate and reliable measurements. The evaluation of electron density was achieved by employing Stark broadening analysis, plasma density and plasma frequency. Additionally, it is worth noting that the Debye length decreases as energy increases. The electron temperature values range from 0.770 eV-0.788 eV. While the electron density ranged from $(4.167-4.688) \times 10^{17}$ cm⁻³. The remaining plasma properties were determined by the utilisation of mathematical formulae and the Boltzmann plot approach. This study provides the first systematic correlation between laser energy 300 mJ-700 mJ and plasma parameters, the temperature and density of electrons, and other fundamental plasma properties in CdO targets, demonstrating a linear increase in electron density with energy. These findings optimise LIBS for Cd detection in environmental monitoring or thin-film diagnostics, utilising emission spectroscopy-based characterisation techniques. This is the first study to quantify Cd plasma parameters across a laser energy range 300 mJ-700 mJ using combined Stark broadening and Boltzmann plot methods.

Keywords: Boltzmann plot method, CdO, LIBS, Stark broadening method, spectroscopy

1. INTRODUCTION

Laser-induced breakdown spectroscopy (LIBS) is used for quantitative and qualitative elemental analysis of liquids, gases and solids. A method of atomic emission spectroscopy called LIBS employs heated vaporisation, dissolution and excitation from laser-generated plasma. The approach has various advantages, the most significant of which is the ability to interrogate material in situ and remotely without any pretreatment since focused optical light forms plasma.² A laser-plasma is shaped onto or into the sample, light is collected from the plasma, and then it is analysed spectroscopically to accomplish LIBS measurement.³ Plasmas generated via laser-solid interactions exhibited with solid objects have a great deal of potential for research in both the theoretical and practical realms. A great number of factors that define the characteristics of the target affect the characteristics of these plasmas. These factors include the properties of the medium in the environment, the pulse duration, the laser wavelength and many others. 4 It can also be employed for LIBS. After the above laser focusing, a plasma plume is produced. The release band for the plasma plume created by the laser can be used to identify the target substance.⁵ Plasma spectroscopy is a diagnostic technique widely used in fundamental scientific fields like astrophysics and plasma physics, as well as in the processing and technology of plasma. Two primary types of plasmas can be distinguished: low-temperature plasmas, called gas discharge plasmas and high-temperature plasmas, which are fusion plasmas. Additionally, it is relevant to basic science domains such as plasma physics and astrophysics.⁶ The measurement of the spectral lines emitted by the hot, dense plasma created at a sample's surface upon exposure to a high-intensity focused laser beam forms the basis of LIBS. LIBS measurements encompass spectrum and time-resolved analyses of the atomic and ionic emission lines produced at a sample's surface following the application of an intense laser pulse. Since the initial use of LIBS for diagnostic applications, numerous systems have been created for both laboratory and field utilisation, capitalising on its distinctive attributes like as rapidity, absence of sample preparation and minimal sample consumption.8 The data obtained from the plasma spectrum allowed for the calculation of the plasma's properties, which ultimately resulted in the synthesis of cadmium (Cd) -rich material during the manufacturing process. These values were shown to have a strong correlation with the material's structure, which was made up of atoms, ions and electrons.9 Laser plasma can be produced from any material, including gases, liquids, solids and aerosols, depending on many factors, including sample properties and detector settings (such as gain and linearity of response). 10 The field of laser-produced plasma emerged with the introduction of powerful lasers. A sample that is exposed to pulsed laser absorbs the energy, heats up, melts and evaporates. Because of the laser's high peak intensity, temperatures can rise to thousands of degrees. The sample ionises at that point, creating plasma.¹¹ The formation of plasma can occur when an abrupt shift in temperature disrupts the electrostatic connections that hold the electrons and nuclei

of an item together. This may occur in the event of a sudden temperature rise. Both the electrons and the nuclei are free to move around in the state of matter known as plasma. The components of a hot gas are, therefore, a composition made up of neutral atoms, electrons and ions in various combinations.¹² The features of the various isolated radiation types as well as the local environment surrounding the radiator define the parameters of plasma radiation. 4 Cadmium oxide (CdO) plasmas are critical for applications in optoelectronics, biological and environmental sensing, yet the energy-dependent dynamics of Cd plasma parameters remain understudied. 13 This work bridges this gap by using emission spectroscopy characterisation techniques to assess the influence of laser energy on LIBS emissions, as well as electron temperature, density and other fundamental plasma parameters defined by electron density (n_e) and electron temperature (T_e.) This work examined the spectra of the major and trace elemental compositions of CdO thin films. The electron temperature and density of the detected plasma were analysed. Time-resolved spectroscopy aids in comprehending the temporal dynamics of the influence of nanostructures on the material matrix.

2. METHODOLOGY

The studied material is Cd from DH Scientific (Erftstsdt, Germany). A Q-switched pulsed laser Nd: YAG with a wavelength of 1,064 nm and a frequency of 6 Hz is used to create the plasma for the experiment, which tests solid targets made of CdO. The plasma was generated this way, an optical fibre with a core diameter of 50 µm was placed 1 cm away from the CdO target surface. to collect the light emission produced by the surface plasma created by the laser. The National Institute of Standards and Technology (NIST) database programme was utilised to allocate the optical emission line to particular elements to ascertain the parameters of the plasma. A charge-coupled device (CCD) spectrometer (model X, resolution Y nm) captured spectra averaged over 50 laser pulses, with a gate delay of 1 µs and an integration time of 100 used to analyse the radiated spectra that had been sent from the samples' surfaces over an optical connection. We did this to find out how different laser intensities affected the plasma's properties setup as depicted in Figure 1.

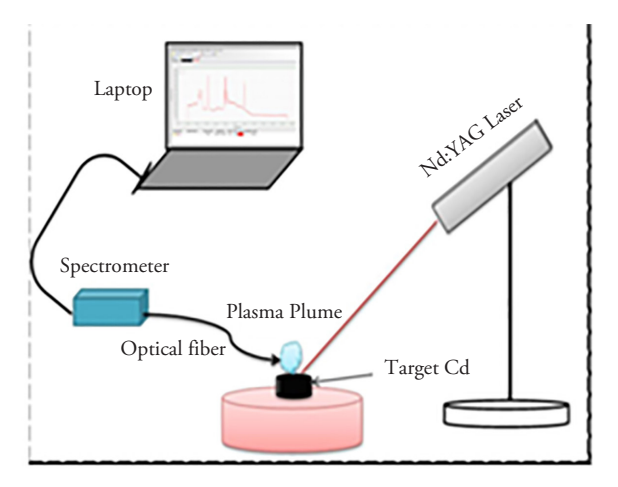


Figure 1: Schematic diagram of the experimental setup for LIBS.

3. RESULTS AND DISCUSSION

3.1 X-ray Diffraction of Simple

X-ray diffraction is a proficient technique for characterising crystalline structure. X-ray diffraction studies provide extensive information regarding orientation and crystal structure, phase, preferential orientation, lattice constants, lattice strain and average crystalline size. If the path difference between two rays diffracted from succeeded atomic layers (with d_{hkl} separation) is a multiple of X-ray wavelength (λ), constructive interference occurs.¹⁵

$$n\lambda = 2 d_{hkl} \sin \theta \tag{1}$$

Where n is an integer number, d is the interlayer distance, λ is the wavelength of the X-ray beam and θ is Bragg's angle.

Scherrer's formula used in crystallite size calculation utilises the broadening of diffraction peaks. 16,17

$$C.S = \frac{k \lambda}{\beta . cos(\theta)}$$
 (2)

For the CuK α transition, λ is the X-ray wavelength employed equivalent to 1.5406 nm, and the full width at half maximum is denoted by β . The shapes factor, k, has a numerical value of 0.90. X-ray diffraction patterns of nanostructured CdO

thin films coated on glass substrates in the range of 20–80 are displayed in Figure 2. Clearly, the film has a cubic structure and is polycrystalline in nature. Also, the five diffraction peaks can be observed and located at 30.9°, 38.99°, 44.49°, 56.42° and 69.99°, corresponding to (311), (200), (422), (531) and (222), crystal planes verify the creation of CdO (JCPDS: 01-104) and (00-5-0640), in that order. Furthermore, the trace of CdO₂ in cubic phase JCPDS is indicated by high peaks at 33.74°, which correspond to (200) planes (CARD NO 39-1221). The small peak at 36.99 corresponds to (031), confirming the formation of Cd(OH)₂ monoclinic JCPDS (CARD NO. 71-2137). The robust apex at 66.64 corresponding to (004) confirm the formation of Cd (JCPDS: 05-0674).^{18,19}

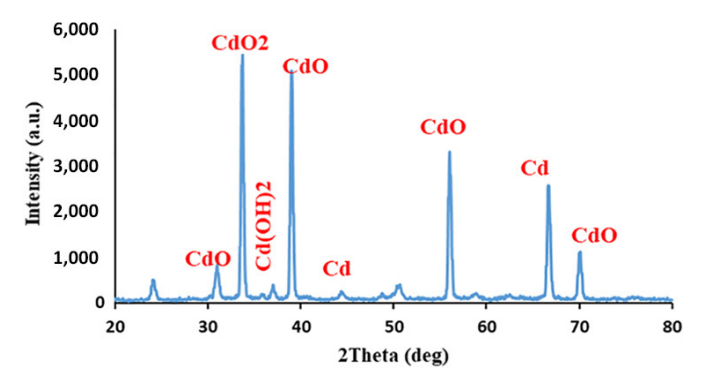


Figure 2: Shows the pure CdO XRD patterns.

This research reviews how laser energy affects the plasma spectra of CdO in the laser ablation process. The main points mentioned in the research can be summarised as follows; The target substance evaporates during the process of transforming the material from a solid or liquid state to a gaseous state due to laser heat. Cloud interaction with the laser beam: The laser beam interacts with the cloud, resulting in its evaporation, heating and plasma formation. Plasma expansion and cooling: The resulting plasma expands and cools over time, which affects the emission spectra that can be measured.

Figure 3 shows the emission spectra of Cd plasma obtained using different laser energies (300 mJ, 500 mJ and 700 mJ). The range of spectral values displayed from 200 nm to 800 nm is the range in which plasma spectra can be measured. The more laser energy there is, at 700 mJ, the Cd I line at 508.58 nm exhibits 2.5× higher intensity than at 300 mJ, indicating enhanced ablation and ionisation. This is due to the increased absorption of the laser by the plasma.²⁰ This results from the increased laser absorption by the target.²¹

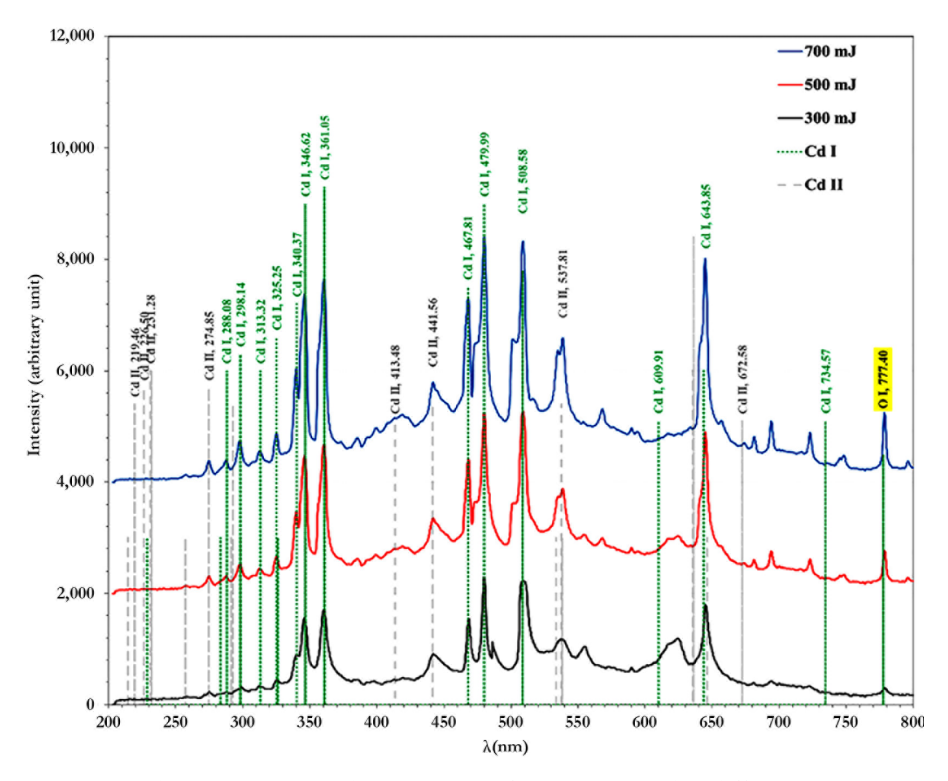


Figure 3: Displays the emission plasma spectra of CdO generated at different laser energies.

Boltzmann plot method for spectral measurements was used to understand ionisation and excitation processes of atoms in plasma; it is essential to know the temperature and species density.²² Estimating. For one line of the same element, the relative density is required. However, the Boltzmann method cannot determine the excitation temperature until local thermal equilibrium (LTE) is achieved. Equation 3 illustrates how electron temperature values are computed by use of the Boltzmann plot technique. This technique needs four peaks from the same ionisation process and atomic species, selected at wavelengths of (325.23, 340.37, 361.05, 479.99, 508,58 and 643.85) nm, with Cd I line as the Cd target.²²

$$\operatorname{Ln}\left(\frac{I_{ji}\lambda_{ji}}{A_{ji}g_{ji}}\right) = \frac{E_j}{k_B T_e} + C \tag{3}$$

Figure 4 shows the Boltzmann plots of ln [(λ _ji I_ji)/(hcA_ji g_j)] as a function of the upper-level energy E_j for the different laser pulse energies. The slope of each linear fit is equal to (-1)/(K_B T_e), from which the electron temperature T_e is obtained. Plasma temperature can be calculated by measuring multiple emission lines simultaneously.²³ Fitting formulae and R² values for all pertinent lines are shown in

Figure 4. (where R^2 is used to indicate linearity strength). In the upper graph, the R^2 value is closer to 1. According to Table 1, the T_e ranges between 0.770 eV and 0.788 eV. As laser energy increases, the mass ablation rate also increases, which raises the T_e . The material's temperature increases with higher laser energy, resulting in enhanced plasma emission and increased kinetic energy, ultimately leading to a higher electron temperature as the plasma absorbs more laser energy. ^{24,25} Electron density can be determined using the linear density, as well as from the line broadening resulting from the Stark effect. ²⁶ According to the Stark effect method outlined in Equation 4, electron density can be calculated. ²⁴

$$n_{e} = \left[\frac{\Delta \lambda_{FWHM}}{2\omega} \right] N_{r} \tag{4}$$

The sharp broadening parameter ω is found to have a full-width theoretical line. Charged species collisions in plasmas produce sharp spectral line widening, which is associated with electron density.

Table 1: The table shows the plasma parameters for Cd at various laser energies

E (mJ)	T _e (eV)	$n_e \times 10^{17} \text{ (cm}^{-3}\text{)}$	$f_p (Hz) \times 10^{10}$	$\lambda_{D} \times 10^{-5} (cm)$	N_D
300	0.770	4.167	5.797	1.010	1799.84
500	0.788	4.557	6.062	0.977	1781.53
700	0.788	4.688	6.148	0.963	1755.47

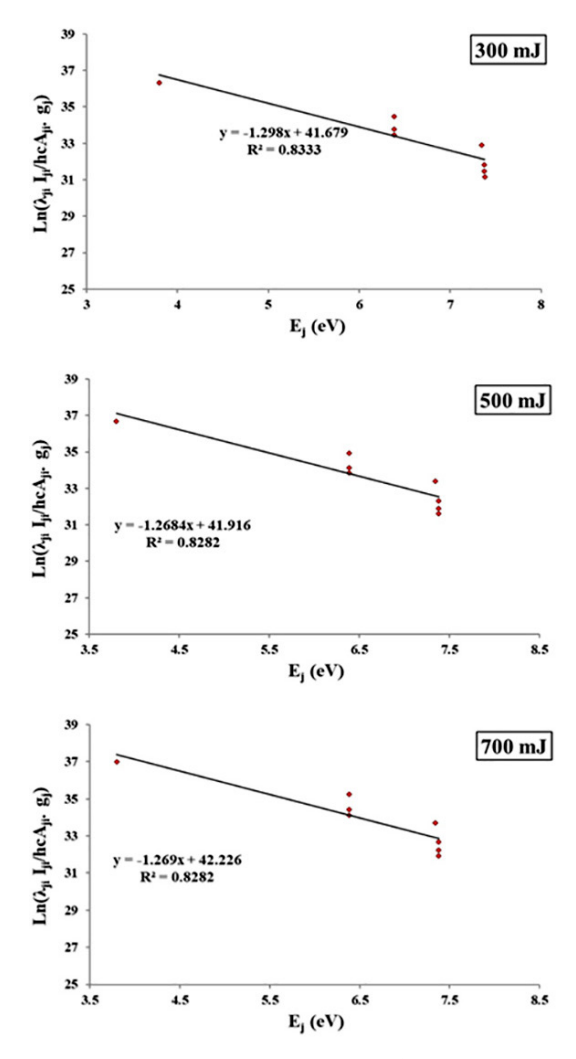


Figure 4: Boltzmann curve illustrating plasma emission from a CdO target at various laser energy levels.

The full width at half maximum (FWHM) of the Cd II emission lines' Starkbroadened profile is shown in Figure 5. Charged particles employ a mechanism called "Debye shielding" to mitigate the impact of nearby electric fields, which gives the plasma its quasi-neutrality. This process allows for formulating the concept of the Debye length (λ_D) .²⁷

$$\lambda_{\rm D} = \sqrt{\frac{\epsilon_0 K_B T_e}{e^2 n e}} \tag{5}$$

The shielding effect can only occur when a substantial number of Debye sphere electrons. The density of electrons and temperature, denoted as N_D , define the number of particles in the Debye sphere, the presence of plasma is further necessitated by $N_D > 1$.

$$N_d = \frac{4\pi}{3} n_e \lambda_D^3 \tag{6}$$

We can assume that electrons provide shielding due to the exponential decay of the potential.²⁰

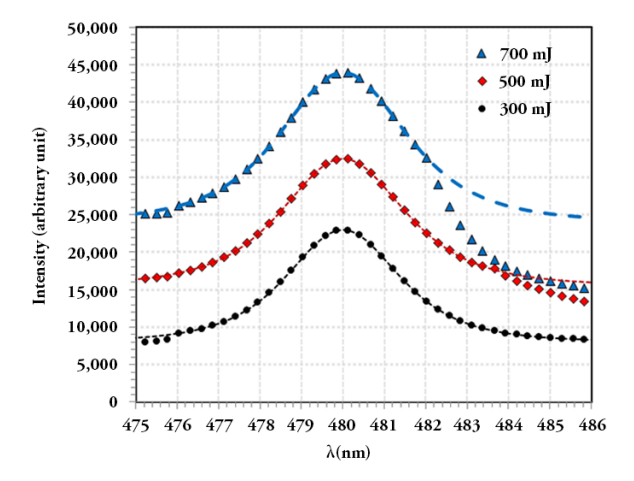


Figure 5: Show Stark broadening effect in CdO plasma at different laser energies.

Figure 6 illustrates the immediate connection between the energy of the laser pulse and the density of electrons (n_e) and the temperature of electrons (T_e). Furthermore, it has been observed that an escalation in laser pulse energy is correlated with an elevation in both (T_e) and (n_e). By reducing the transmission of high-intensity laser energy along the laser beam's path, plasma shielding is a technique. This might explain the increase in plasma temperature. Additionally, the plasma may block the laser beam's path when it strikes the target resulting in opacity.²⁸

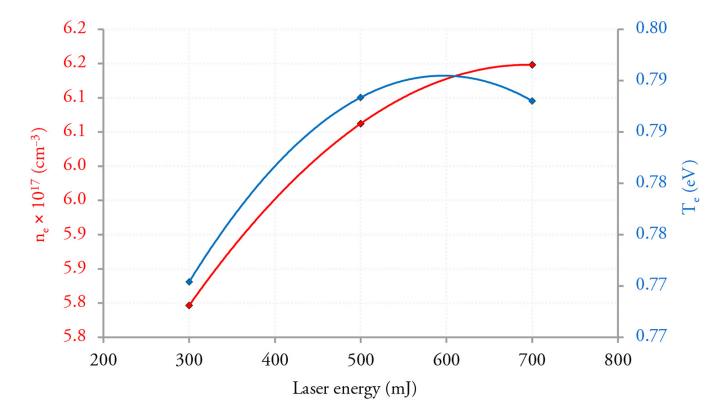


Figure 6: Illustrates how (T_c) and (n_c) change in relation to laser energy.

It has been observed that when the energy of the laser pulse grows, the Debye length (λ_D) diminishes. This occurs because lasers have varying effects on plasma based on their frequency and intensity. Usually, increasing the laser pulse's energy raises the material's temperature (T_e) enough to separate the outermost electron from the atom, which leads to a large rise in electron density. Therefore, the λ_D has an inverse relationship with the $(n_e)^{1/2}$. This means that as n_e goes down, so does the λ_D , and so does the (N_D) in the Debye sphere. In addition, uncertainties in T_e (± 0.02 eV) and ne (± 0.3 \times 10 17 cm $^{-3}$) arise from laser energy fluctuations (± 5%) and spectral fitting error. The observed phenomena can be attributed to the fluctuations in massablation rates and photoionisation relative to the examined pulse energy. The results gained investigate the potential to regulate certain plasma parameters, applicable in several domains of material science, spectroscopic research and plasma interaction dynamics control.

4. CONCLUSION

In conclusion, this work conducted an extensive examination of plasma properties in a CdO target using LIBS, specifically emphasising the influence of different laser intensities. Through systematic experimentation and meticulous data analysis, we have gained valuable insights into the intricate relationship between laser energy and the resulting plasma characteristics. Through a precise analysis of the data, we were able to interpret the relationship between changes in laser energy and its effects on plasma parameters such as electron temperature and density. We observed numerous Cd emission lines in the plasma spectra. The results indicated that increasing the amount of laser energy used in sample production leads to an increase in plasma intensity. Additionally, exploring a wider range of laser energies and conducting in-depth computational simulations could offer a more comprehensive picture of

the underlying mechanisms governing the laser-plasma interaction. This discrepancy results from variations in the components. The linear rise in T_e and n_e with laser energy (300 mJ–700 mJ) enables precise tuning of Cd plasma conditions for LIBS-based quantification in industrial Cd waste analysis. The inverse relationship between λ_D and n_e confirms Debye shielding dominance at higher energies. Findings directly apply to LIBS optimisation for cadmium detection in environmental pollutants or CdO thin-film quality control. The results of this work have substantial practical ramifications for domains such as surface alteration, LIBS and material investigation. Additionally, they contribute to our fundamental understanding of plasma dynamics.

5. ACKNOWLEDGEMENTS

We would like to thank the University of Baghdad, College of Science for women, Department of Physics, Postgraduate Laboratory for Medical Physics for ensuring the availability of all research facilities.

6. REFERENCES

- 1. Sarkar, A. & Singh, M. (2017). Laser-induced plasma electron number density: Stark broadening method versus the Saha–Boltzmann equation. *Plasma Sci. Technol.*, 19(2), 025403. https://doi.org/10.1088/2058-6272/19/2/025403
- 2. Mazhir, S. N. (2018). Spectroscopic study of (TiO₂)_{1-x}(CuO)_x plasma generated by Nd: YAG laser. *ARPN J. Eng. Appl. Sci.*, 13(3), 864–869.
- 3. Harb, N. H. et al. (2024). Preparation and characterisation of CdO@Au nanoparticles by hybrid system using laser ablation and plasma jet methods for cytotoxicity against rat embryonic fibroblast cell line. *J. Phys. Sci.*, 35(3), 17–25. https://doi.org/10.21315/jps2024.35.3.2
- 4. Chen, F. F. (1974). Introduction to Controlled Fusion. In *Introduction to Plasma Physics*. Springer, 279–318. https://doi.org/10.1007/978-1-4757-0459-4_9
- 5. Tawfik, W. F. et al. (2013). Characterization and analysis of nanostructured CdO thin film using LIBS technique. *2013 Saudi Int. Electron. Commun. Photonics Conf.*, 1–5. https://doi.org/10.1109/SIECPC.2013.6550798
- 6. Yao, H. et al. (2020). Investigation into the effect of increasing target temperature and the size of cavity confinements on laser-induced plasmas. *Metals*, 10(3), 393. http://dx.doi.org/10.3390/met10030393
- 7. Buddin, M. M. H. et al. (2017). Kinetic study of Cd(II) ions extraction using trioctylamine as carrier in bulk liquid membrane (BLM). *J. Phys. Sci.*, 30(2), 157–168. https://doi.org/10.21315/jps2019.30.2.9
- 8. Fikry, M. et al. (2020). Investigation on the effects of laser parameters on the plasma profile of copper using picosecond laser induced plasma spectroscopy. *Opt. Quant. Electron.*, 52, 249. https://doi.org/10.1007/s11082-020-02381-x

- 9. Fikry, M. et al. (2023). Spectroscopic determination of the Stark broadening parameters of Al (I) 305.007 nm in atmospheric air using picosecond time-resolved LIPS. *J. Mole. Struct.*, 1276, 134796. https://doi.org/10.1016/j.molstruc.2023.134796
- 10. Mazhir, S. N. et al. (2018). Effects of gas flow on spectral properties of plasma jet induced by microwave. *Baghdad Sci. J.*, 15(1), 81–86. https://doi.org/10.21123/bsj.2018.15.1.0081
- 11. Muryoush, A. Q. et al. (2019). Effect of cold plasma on histological compositions of the rabbits fracture bone tissue. *Iraqi J. Sci.*, 60(9), 1997–2002. https://doi.org/10.24996/ijs.2019.60.9.12
- 12. Salih, A. A. et al. (2021). Preparation and characterizations of nanomaterial by pulsed laser ablation in liquid (PLAIL) as friendly environment paint. *J. Phys. Conf. Ser.*, 1795(1), 012023. https://doi.org/10.1088/1742-6596/1795/1/012023
- 13. Mohanraj, K. et al. (2017). Structural, optical and electrical properties of green synthesis CdO nanoparticles and its Ag/CdO/P-Si junction diode fabricated via JNS pyrolysis technique. *Int. J. Thin. Fil. Sci. Tec.*, 6(2), 87–91. https://doi.org/10.18576/ijtfst/060207
- 14. National Institute of Standards and Technology (NIST) (2017). Atomic spectra database. *NIST*. https://dx.doi.org/10.18434/T4W30F
- 15. Ibrahim, I. M. et al. (2019). Enhancement the sensitivity of CdS nano structure by adding of rare earth materials. *J. Phys. Conf. Ser.*, 1178, 012013. https://doi.org/10.1088/1742-6596/1178/1/012013
- Gudla, U. R. et al. (2021). Structural, optical and luminescence properties of pure, Fe-doped and glucose-capped CdO Semiconductor nanoparticles for their antibacterial activity. J. Mater. Sci. Mater. Electron., 32, 3920–3928. https://doi.org/10.1007/ s10854-020-05135-3
- 17. Rajaboopathi, S. & Thambidurai, S. (2017). Heterostructure of CdO-ZnO nanoparticles intercalated on PANI matrix for better thermal and electrochemical performance. *Mater. Sci. Semicond. Process.*, 59, 56–67. https://doi.org/10.1016/j.mssp.2016.11.040
- 18. Kumar, T. et al. (2024). Rapid authentication and evaluation of minerals in milk powder using laser-induced breakdown spectroscopic (LIBS) technique. *J. Opt.*, 53, 1243–1255. https://doi.org/10.1007/s12596-023-01265-z
- 19. Elashry, S. et al. (2024). Surface activation of viscose textiles via air, argon, and oxygen dielectric barrier discharge plasma: influence of peak voltage. *Plasma Sci. Technol.*, 26(7), 075508. https://doi.org/10.1088/2058-6272/ad370b
- 20. Ibrahim, I. M. et al. (2019). Enhancement the sensitivity of CdS nano structure by adding of rare earth materials. *J. Phys. Conf. Ser.*, 1178, 012013. https://doi.org/10.1088/1742-6596/1178/1/012013
- 21. Yahya, K. A. (2021). Enhancement of electron temperature under dense homogenous plasma by pulsed laser beam. *Baghdad Sci. J.*, 18(4), 1344–1349. https://doi.org/10.21123/BSJ.2021.18.4.1344
- 22. Mohamed, F. K. & Al-Rashid, S. N. (2017). Nano coating designs of ruby laser resonators. *Dig. J. Nanomater. Biostruct.*, 12(3), 933–939.

- 23. Majeed, N. F. et al. (2025). Effect of laser pulses (Nd:YAG) 1064 nm on the physical properties of alum and turmeric extracts and antibacterial efficacy. *J. Opt.* https://doi.org/10.1007/s12596-025-02748-x
- 24. Fahad, O. A. et al. (2025). High-performance ZnO/CdTe/Ge/Si heterojunction photodetector for short/mid-wavelength detection. *Sens. Actuators A Phys.*, 383, 116198. https://doi.org/10.1016/j.sna.2025.116198
- 25. Abed, H. A. et al. (2023). The optical and structural properties of the Fe@Au core—shell nanoparticles prepared by PLAL. *Inter. J. Nanosc.*, 22(6), 2330005. https://doi.org/10.1142/S0219581X23300055
- 26. Ohno, N. et al. (2006). Validity of electron temperature measurement by using Boltzmann plot method in radio frequency inductive discharge in the atmospheric pressure range. *Plasma Fusi. Res.*, 1, 028. https://doi.org/10.1585/pfr.1.028
- 27. Fadhil, H. M. et al. (2022). Structural and spectroscopic analysis for silver bulk and nanoparticles. *Karbala Int. J. Modern Sci.*, 8(2), 5. https://doi.org/10.33640/2405 -609X.3220
- 28. Hamad, T. K. et al. (2019). Characterizing laser-induced plasma generated from MgO/PVA solid targets. *Opt. Spectrosc.*, 127, 153–158. https://doi.org/10.1134/S0030400X19070099T